Hepatic insulin resistance in mice with hepatic overexpression of diacylglycerol acyltransferase 2

François R. Jornayvaz[a], Andreas L. Birkenfeld[a], Michael J. Jurczak[a,b], Shoichi Kanda[a], Blas A. Guigni[a], Debbie C. Jiang[a], Dongyan Zhang[a,b], Hui-Young Lee[a,b], Varman T. Samuel[a], and Gerald I. Shulman[a,b,c,1]

Departments of [a]Internal Medicine and [c]Cellular and Molecular Physiology and [b]Howard Hughes Medical Institute, Yale University School of Medicine, New Haven, CT 06536

Contributed by Gerald I. Shulman, March 2, 2011 (sent for review January 14, 2011)

Mice overexpressing acylCoA:diacylglycerol (DAG) acyltransferase 2 in the liver (Liv-*DGAT2*) have been shown to have normal hepatic insulin responsiveness despite severe hepatic steatosis and increased hepatic triglyceride, diacylglycerol, and ceramide content, demonstrating a dissociation between hepatic steatosis and hepatic insulin resistance. This led us to reevaluate the role of DAG in causing hepatic insulin resistance in this mouse model of severe hepatic steatosis. Using hyperinsulinemic-euglycemic clamps, we studied insulin action in Liv-*DGAT2* mice and their wild-type (WT) littermate controls. Here, we show that Liv-*DGAT2* mice manifest severe hepatic insulin resistance as reflected by decreased suppression of endogenous glucose production (0.8 ± 41.8 vs. 87.7 ± 34.3% in WT mice, $P < 0.01$) during the clamps. Hepatic insulin resistance could be attributed to an almost 12-fold increase in hepatic DAG content ($P < 0.01$) resulting in a 3.6-fold increase in protein kinase Cε (PKCε) activation ($P < 0.01$) and a subsequent 52% decrease in insulin-stimulated insulin receptor substrate 2 (IRS-2) tyrosine phosphorylation ($P < 0.05$), as well as a 64% decrease in fold increase pAkt/Akt ratio from basal conditions ($P < 0.01$). In contrast, hepatic insulin resistance in these mice was not associated with increased endoplasmic reticulum (ER) stress or inflammation. Importantly, hepatic insulin resistance in Liv-*DGAT2* mice was independent of differences in body composition, energy expenditure, or food intake. In conclusion, these findings strengthen the link between hepatic steatosis and hepatic insulin resistance and support the hypothesis that DAG-induced PKCε activation plays a major role in nonalcoholic fatty liver disease (NAFLD)-associated hepatic insulin resistance.

protein kinase Cε | ceramides, insulin receptor kinase | type 2 diabetes

Hepatic insulin resistance associated with nonalcoholic fatty liver disease (NAFLD) is a major risk factor for the development of type 2 diabetes (1–6). However, whether there is a causal link between NAFLD and hepatic insulin resistance remains controversial (7, 8). Although intracellular triglyceride is unlikely to be the direct mediator of insulin resistance (3, 4), other related intracellular lipid intermediates such as diacylglycerol (3, 4, 9–12) and ceramide (13) have been postulated to block insulin signaling at the level of the insulin receptor kinase and Akt2, respectively, leading to insulin resistance. Indeed, diacylglycerol (DAG) has been shown to activate protein kinase Cε (PKCε) in the liver, which in turn binds to the insulin receptor and inhibits its tyrosine kinase activity (14).

However, a recent paper reported that mice overexpressing acylCoA:diacylglycerol acyltransferase 2 (Liv-*DGAT2*) in the liver were not insulin resistant despite severe hepatic steatosis associated with increased liver DAG content (15). This study was of critical importance because it dissociated hepatic DAG content from hepatic insulin resistance and implied that hepatic DAG was not a causal factor in hepatic insulin resistance. This apparent paradox led us to reconsider the role of hepatic DAG in causing hepatic insulin resistance in this mouse model of severe hepatic steatosis. Detailed studies were performed to evaluate insulin responsiveness in conscious mice by using the hyperinsulinemic-euglycemic clamp technique combined with radio-labeled glucose to assess rates of whole body glucose turnover. In addition, we also assessed tissue lipid intermediates that have been associated with insulin resistance by liquid chromatography (LC)-tandem mass spectrometry as well as signaling events typically associated with an increase in liver DAG content, i.e., PKCε activation as well as potential alterations in insulin signaling downstream of the insulin receptor kinase. Finally, given the well-established associations between endoplasmic reticulum (ER) stress (16–18) and inflammation (16, 17, 19, 20) with hepatic steatosis, we also assessed these pathways in this mouse model.

Results

Liv-*DGAT2* Mice Manifest Severe Hepatic Insulin Resistance. To assess hepatic and peripheral insulin sensitivity, we performed hyperinsulinemic-euglycemic clamps 6 to 7 d after surgery, when mice fully recovered their presurgery body weights (Table 1). Glucose infusion rates required to maintain euglycemia (Fig. 1*A*) during the clamps were 42% lower in Liv-*DGAT2* mice compared with wild-type (WT) mice, demonstrating whole body insulin resistance in the Liv-*DGAT2* mice (Fig. 1*B*). Although basal endogenous glucose production was not different between groups (Fig. 1*C*), endogenous glucose production during the hyperinsulinemic-euglycemic clamp was ∼10-fold higher in Liv-*DGAT2* mice (Fig. 1*D*), reflecting severe hepatic insulin resistance (Fig. 1*E*). Insulin-stimulated whole body glucose disposal (Fig. 1*F*) was similar between genotypes, reflecting the hepatic predominance of insulin resistance in Liv-*DGAT2* mice. Insulin-stimulated whole body glycolysis (Fig. 1*G*) and glycogen synthesis (Fig. 1*H*) were similar between groups. Importantly, plasma insulin concentrations were similar between WT and Liv-*DGAT2* mice at the end of the clamps (Table 1). Although there was a trend toward reduced basal plasma fatty acid concentrations in Liv-*DGAT2* mice, the ability of insulin to decrease plasma fatty acid concentrations during the hyperinsulinemic-euglycemic clamps was also significantly impaired in Liv-*DGAT2* mice (Table 1), suggesting that insulin suppression of white adipose tissue lipolysis was also decreased in these mice. Importantly, no potentially confounding factors such as differences in body composition, energy expenditure, food intake, or activity interfered in the metabolic evaluation of these mice. Indeed, all these parameters were similar between Liv-*DGAT2* mice and their littermate WT controls except the respiratory quotient of Liv-*DGAT2* mice that was lower than their WT littermates during light hours (Table 1), i.e., during sleep, suggesting an increase in lipid oxidation during fasting. Finally,

Author contributions: F.R.J. and G.I.S. designed research; F.R.J., A.L.B., M.J.J., S.K., B.A.G., D.C.J., D.Z., H.-Y.L., V.T.S., and G.I.S. performed research; F.R.J., A.L.B., M.J.J., S.K., B.A.G., D.C.J., D.Z., H.-Y.L., V.T.S., and G.I.S. analyzed data; and F.R.J., A.L.B., M.J.J., S.K., B.A.G., D.C.J., D.Z., H.-Y.L., V.T.S., and G.I.S. wrote the paper.

The authors declare no conflict of interest.

Freely available online through the PNAS open access option.

[1]To whom correspondence should be addressed. E-mail: gerald.shulman@yale.edu.

This article contains supporting information online at www.pnas.org/lookup/suppl/doi:10.1073/pnas.1103451108/-/DCSupplemental.

Table 1. Physiologic parameters and plasma analyses

Physiological parameters	WT	Liv-*DGAT2*
Body weight (g)	25.2 ± 0.3	24.8 ± 0.4
Lean mass (% of body weight)	71.2 ± 0.7	72.2 ± 0.7
Fat mass (% of body weight)	10.6 ± 0.8	9.6 ± 0.7
Energy expenditure [kcal/(kg-h)]	18.2 ± 0.4	18.8 ± 0.4
Caloric intake [kcal/(kg-h)]	17.5 ± 1.9	13.9 ± 2.1
Activity (counts/h)	136.9 ± 21.2	130.7 ± 15.3
RQ during light hours	0.89 ± 0.01	0.86 ± 0.01*
RQ during dark hours	0.95 ± 0.01	0.95 ± 0.01
Recovery from presurgery BW (%)	101.8 ± 1.8	102.6 ± 2.4
Plasma analyses		
Fasting insulin (μU/mL)	16.3 ± 4.4	14.5 ± 2.5
Clamp insulin (μU/mL)	53.1 ± 8.3	47.6 ± 7.2
Fasting FA (mEq/L)	1.1 ± 0.4	0.5 ± 0.2
Insulin-stimulated FA (mEq/L)	0.5 ± 0.2	0.4 ± 0.2
Insulin suppression of FA (%)	56.5 ± 9.2	32.6 ± 19.6*
Triglycerides (mg/dL)	87.5 ± 10.1	65.7 ± 11.4
Total cholesterol (mg/dL)	141.9 ± 9.9	134.7 ± 13.0
High-density lipoprotein cholesterol (mg/dL)	80.8 ± 4.8	56.4 ± 10.5
Interleukin-1β (pg/mL)	6.2 ± 1.6	12.6 ± 3.7
IFN-γ (pg/mL)	3.4 ± 0.3	3.3 ± 0.4
Interleukin-6 (pg/mL)	18.5 ± 2.2	23.4 ± 8.0
Interleukin-10 (pg/mL)	58.2 ± 6.6	48.7 ± 1.8
Tumor necrosis factor-α (pg/mL)	15.3 ± 6.4	8.1 ± 1.3

BW, body weight; FA, fatty acids; RQ, respiratory quotient. *$P < 0.05$ vs. WT. Data are represented as mean ± SEM.

plasma measurements showed no difference in triglycerides and total cholesterol concentrations between genotypes (Table 1). However, Liv-*DGAT2* mice had a trend toward lower high-density lipoprotein (HDL) cholesterol concentrations ($P = 0.08$, Table 1).

Liv-*DGAT2* Mice Have Increased Hepatic Lipid Intermediates and Impaired Hepatic Insulin Signaling. Hepatic lipid intermediates, triglycerides (Fig. 2*A*), cytosolic DAG (Fig. 2*B*), and ceramide (Fig. 2*C*) were all significantly increased in Liv-*DGAT2* mice. The increase in hepatic DAG content was associated with a significant increase in PKCε activation (Fig. 2*D*) and a subsequent 52% decrease in insulin-stimulated insulin receptor substrate 2 (IRS-2) tyrosine phosphorylation (Fig. 2*E*), confirming the insulin resistance of Liv-*DGAT2* mice downstream of the insulin receptor. Moreover, the fold increase from basal to insulin-stimulated conditions of pAkt/Akt ratio was ∼64% lower (Fig. 2*F*) in Liv-*DGAT2* mice compared with the WT littermates, confirming hepatic insulin resistance.

Hepatic Insulin Resistance in Liv-*DGAT2* Mice Is Not Associated with ER Stress and Inflammation. ER stress and inflammation have also been suggested as alternative hypotheses to explain hepatic insulin resistance (16–20). We therefore examined several markers of these pathways, complementary to previously reported ones in this mouse model (15). Hepatic protein levels of C/EBP homologous protein (CHOP) (Fig. 3*A*), IgH chain binding protein (BIP) (Fig. 3*B*), and phospho-eIF2α (Fig. 3*C*), three important markers of ER stress, were similar between groups, as were phosphorylated and total JNK, PKR-like ER kinase, and NFκB (15). Additionally, concentrations of plasma cytokines (IL-1β, IL-6, IFN-γ, interleukin-10, and TNF-α) were not different between Liv-*DGAT2* and WT mice (Table 1). Finally, microscopy did not reveal significant inflammation in WT and Liv-*DGAT2* mice, but showed predominantly macrovesicular steatosis in Liv-*DGAT2* mice (Fig. 3*D*). Taken together, these results suggest that neither ER stress nor inflammation were the cause of hepatic insulin resistance in this mouse model of NAFLD.

Liv-*DGAT2* Mice Have Increased Hepatic Lipid Synthesis Gene Expression. Consistent with their genotype, we found that Liv-*DGAT2* mice had an increase in the hepatic expression of DGAT2 mRNA (Fig. S1). However, contrary to what would be expected from the function of DGAT2, these mice not only had an increase in liver triglycerides, but also in liver DAG as previously described (15). This is probably secondary to a compensatory mechanism leading to an increase in hepatic levels of sterol regulatory element binding protein 1c (SREBP-1c) mRNA (Fig. S1), a master regulatory transcription factor in lipid synthesis (21). There were no differences in hepatic fibroblast growth factor 21 (FGF21) and carnitine palmitoyltransferase 1 (CPT1) mRNA levels (Fig. S1), which both encode proteins that promote lipid oxidation, confirming the predominance of hepatic lipid synthesis in promoting hepatic steatosis in Liv-*DGAT2* mice.

Discussion

Mice with hepatic overexpression of DGAT2 have been shown to have normal hepatic insulin responsiveness despite severe hepatic steatosis and increases in hepatic DAG content (15). This was a critically important observation because it implied that hepatic DAG content was not a causal factor in the pathogenesis of NAFLD-associated hepatic insulin resistance and has been widely cited as strong evidence against the DAG hypothesis for lipid-induced hepatic insulin resistance (22–29). This study therefore led us to reevaluate the role of hepatic DAG content and other lipid intermediates in causing hepatic insulin resistance in this mouse model of severe hepatic steatosis. Contrary to the findings of Monetti et al. (15), we found that Liv-*DGAT2* mice had profound hepatic insulin resistance, which was associated with an almost 12-fold increase in hepatic cytosolic DAG content leading to PKCε activation, resulting in decreased insulin signaling at the level of IRS-2 tyrosine phosphorylation. Moreover, we also found a lower fold increase in pAkt/Akt ratio from basal to insulin-stimulated conditions in Liv-*DGAT2* mice, providing additional evidence of impaired insulin signaling downstream of the insulin receptor, consistent with hepatic insulin resistance displayed by these mice. Hepatic ceramide content was also slightly increased (∼8%), which may have also contributed to the hepatic insulin resistance observed in this mouse model of severe hepatic steatosis.

Although we chose a slightly different experimental protocol than Monetti et al. (15), it is unclear why our hyperinsulinemic-euglycemic clamp results differ from theirs. It is possible that differences in the conditions and timing of the clamp studies may explain these discrepancies. Monetti et al. (15) performed their hyperinsulinemic-euglycemic clamp studies using an insulin infusion rate of 2.0 mU/(kg-min) in mice 3 d postoperatively, which may not have been enough time for the mice to fully recover from their surgery. In contrast, we performed our hyperinsulinemic-euglycemic clamp studies using an insulin infusion rate of 3.0 mU/(kg-min) in mice 6 to 7 d postoperatively when the mice had fully recovered to their presurgical body weights, following standard operating procedures (30). Consistent with the hypothesis, Monetti et al. (15) did not observe any suppression of endogenous glucose production during their hyperinsulinemic-euglycemic clamps in their WT control mice, whereas we observed ∼88% suppression of endogenous glucose production in WT mice during our hyperinsulinemic-euglycemic clamp studies. Importantly, our clamp studies were done on a similar regular chow diet following a similar fasting time (6 h) as well as at similar ages (3–4 mo) as performed by Monetti et al. (15). Also, we used the same Liv-*DGAT2* mice and bred them in similar conditions as Monetti et al. (15).

This study mirrors the results found when rats are treated with a DGAT2 antisense oligonucleotide (ASO) to knock down hepatic protein expression of DGAT2 (31). In this study, DGAT2 ASO-treated rats showed improved hepatic insulin sensitivity, which could be attributed to a reduction in liver DAG content and

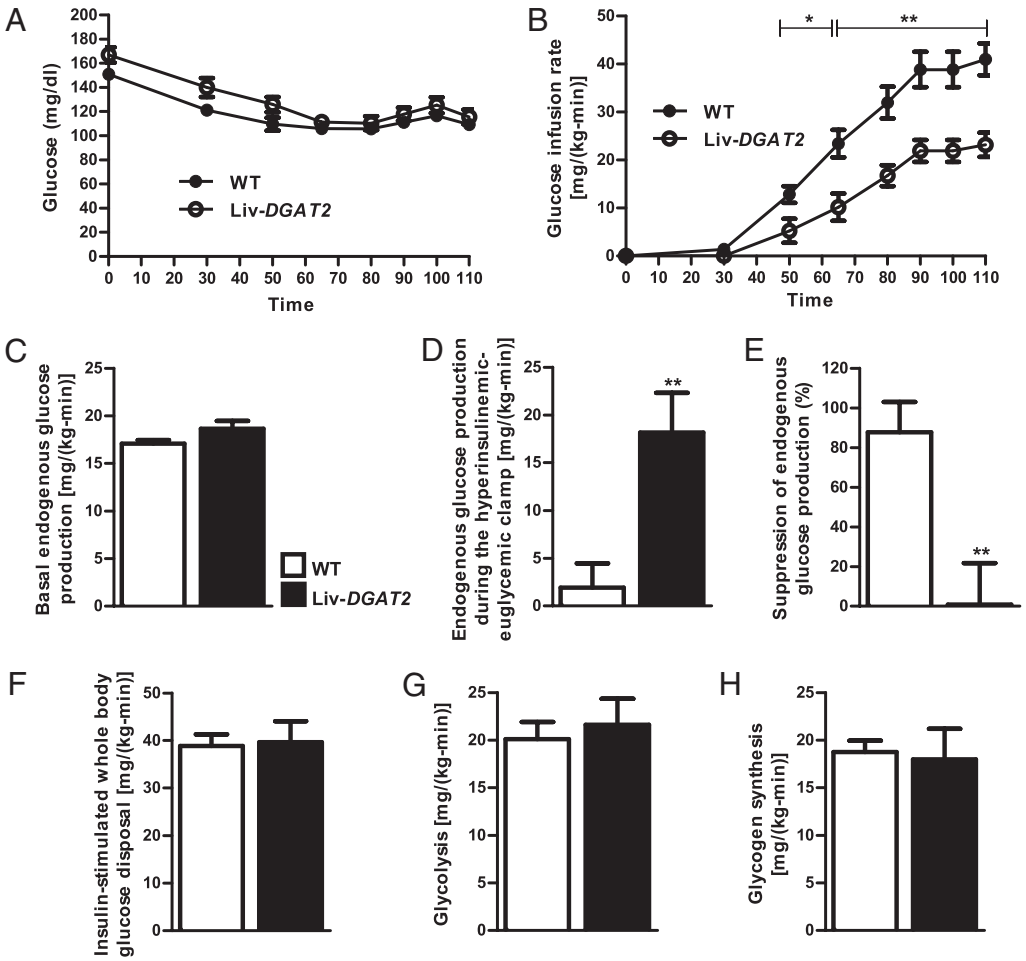

Fig. 1. Liv-*DGAT2* mice have severe hepatic insulin resistance. (*A*) Glucose time course during the hyperinsulinemic-euglycemic clamps. (*B*) Glucose infusion rates during the clamps. (*C*) Basal endogenous glucose production. (*D*) Endogenous glucose production during the hyperinsulinemic-euglycemic clamp. (*E*) Suppression of endogenous glucose production during the hyperinsulinemic-euglycemic clamps. (*F*) Insulin-stimulated whole-body glucose disposal. (*G*) Glycolysis. (*H*) Glycogen synthesis. $*P < 0.05$ and $**P < 0.01$ vs. WT mice. Data are represented as mean ± SEM.

decreased PKCε activation, leading to an increase in insulin-stimulated IRS-2 tyrosine phosphorylation. DGAT2 ASO-treated rats not only displayed a reduction in liver DAG content, but also a reduction in liver triglyceride content, which could be attributed to decreased hepatic SREBP-1c mRNA expression, mirroring again the opposite findings we found in Liv-*DGAT2* mice.

In contrast to the large increases in hepatic cytosolic DAG content and PKCε activation, we did not find any difference in markers of hepatic ER stress or inflammation, which is consistent with Monetti et al. (15), and suggests that these pathways are not likely contributing to the hepatic insulin resistance observed in this mouse model of NAFLD.

DGAT2 overexpression in the liver leads to an expected increase in hepatic triglyceride content but also surprisingly to an increase in hepatic DAG content. This may be secondary to a compensatory mechanism up-regulating lipid synthesis to provide substrates for the conversion of DAGs to triglycerides. Consistent with this hypothesis, we observed an increased hepatic expression of SREBP-1c mRNA levels. Alternatively, it is possible that DGAT2 can also run in the opposite direction, i.e., convert triacylglycerols to diacylglycerols, which may function to avoid hepatic overload of triglycerides but secondarily lead to increased hepatic DAG content. Although both Monetti et al. (15) and we found higher hepatic content of triglycerides, DAGs, and ceramides in Liv-*DGAT2* mice, it is difficult to make a head-to-head comparison of the levels of each lipid intermediate as the methods used to assess the latter were different, as were the units to express them. However, the ratios of each lipid metabolite between Liv-DGAT2 and WT mice were similar between our study and the study by Monetti et al. (15). For example, they report a fivefold increase in liver triglyceride content, whereas we found a slightly lower, i.e., threefold increase in liver triglyceride content. However, contrary to the findings of Monetti et al., we did not find significant differences in plasma triglyceride concentrations between the two groups.

In conclusion, the present study demonstrates that mice specifically overexpressing DGAT2 in the liver have profound hepatic insulin resistance. This could be attributed to an increase in hepatic DAG content, leading to PKCε activation and subsequent impaired insulin signaling. In contrast, ER stress or inflammation do not appear to be playing major roles in causing hepatic insulin resistance in this mouse model of severe hepatic steatosis. Taken together, these findings support the hypothesis that DAG-induced PKCε activation plays a key role in NAFLD-associated hepatic insulin resistance.

Materials and Methods

Animals and Diets. Male Liv-*DGAT2* mice (lower expression level) were a generous gift from Dr. Robert Farese, Jr. (University of California, San Francisco, CA). The mice were generated as previously described (15) using a C57BL/6NHsd background and individually housed in a pathogen-free barrier facility under controlled temperature (23 °C) and lighting (12:12 h

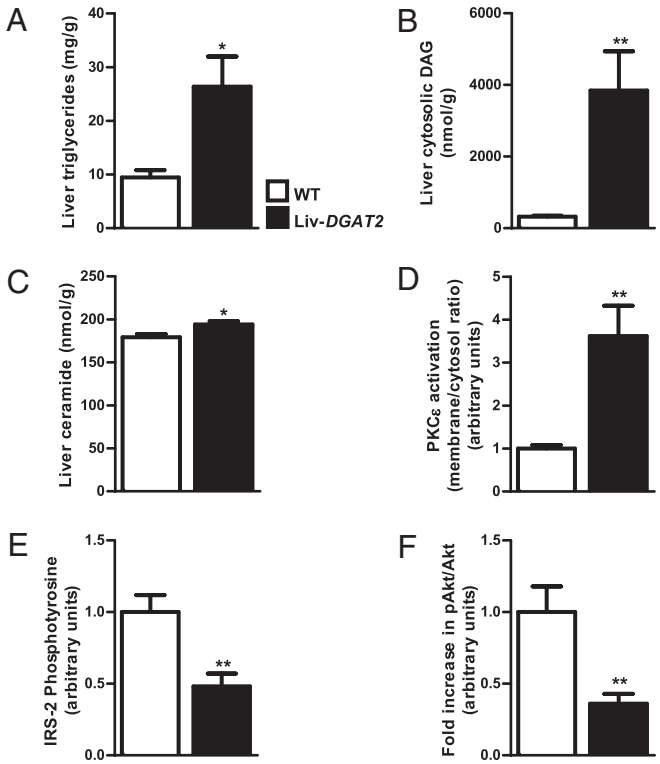

Fig. 2. Increased hepatic lipid metabolites and impaired hepatic insulin signaling in Liv-*DGAT2* mice. (*A*) Liver triglycerides. (*B*) Cytosolic DAG content. (*C*) Ceramide content. (*D*) PKCε activation in Liv-*DGAT2* mice. (*E*) Decreased insulin-stimulated IRS-2 tyrosine phosphorylation in Liv-*DGAT2* mice. (*F*) Lower fold increase in pAkt/Akt ratio from basal to insulin-stimulated conditions in Liv-*DGAT2* mice. $*P < 0.05$ and $**P < 0.01$ vs. WT mice. Data are represented as mean ± SEM.

light/dark cycle, lights on at 7:00 AM). Liv-*DGAT2* mice were then bred at Yale University, as previously described (15). Mice had free access to water and food (regular rodent chow diet, 2018S; Harlan Teklad). The proportions of calories derived from nutrients were as follows: 17% fat, 60% carbohydrate, 23% protein, energy density 3.3 kcal/g. Body composition was assessed by ^{1}H magnetic resonance spectroscopy using a Bruker Minispec analyzer. Metabolic parameters and physical activity were measured using the Oxymax system from Columbus Instruments. All experiments were done in 6-h fasted animals (6:00 AM to noon) at 3–4 mo of age. All procedures were approved by the Yale University Animal Care and Use Committee.

Hyperinsulinemic-Euglycemic Clamp Studies. A jugular venous catheter was implanted 6 to 7 d before the hyperinsulinemic-euglycemic clamps. To assess basal whole-body glucose turnover, [3-^{3}H]-glucose (HPLC purified; Perkin-Elmer Life Sciences) was infused at a rate of 0.05 μCi/min for 120 min into the jugular catheter. Following the basal period, hyperinsulinemic-euglycemic clamps were conducted in conscious mice for 110 min with a 4 min primed (29 mU/kg) followed by a continuous [3 mU/(kg-min)] infusion of human insulin (Novolin; Novo Nordisk), a continuous infusion of [3-^{3}H]-glucose (0.1 μCi/min), and a variable infusion of 20% dextrose to maintain euglycemia (100–120 mg/dL). Plasma samples were obtained from the tip of the tail at 0, 30, 50, 65, 80, 90, 100, and 110 min. The tail incision was made at least 2 h before the first blood sample was taken to allow for acclimatization, according to standard operating procedures (30). Also, mice received an i.v. albumin-containing solution mimicking artificial plasma during the insulin-stimulated period of the clamp to compensate for volume loss secondary to blood sampling. At the end of the clamps, mice were anesthetized with pentobarbital sodium injection (150 mg/kg) and all tissues were taken within 4 min, snap-frozen in liquid nitrogen, and stored at −80 °C for subsequent analysis.

Biochemical Analysis and Calculations. Plasma glucose (10 μL per sample) was measured using a YSI 2700D glucose analyzer. Plasma fatty acids were determined with the NEFA C kit (Wako Pure Chemical Industries). Plasma insulin concentrations were measured by a RIA kit (Millipore). Triglycerides and cholesterol panel were analyzed using COBAS Mira Plus (Roche). Plasma cytokines were measured using a mouse multiplex assay kit (Meso Scale Discovery). For the determination of ^{3}H-glucose, plasma was deproteinized with $ZnSO_4$ and $Ba(OH)_2$, dried to remove ^3H_2O, resuspended in water, and counted in scintillation fluid (Ultima Gold; Perkin-Elmer Life Sciences).

Rates of basal and insulin-stimulated whole-body glucose turnover were determined as the ratio of the [3-^{3}H]-glucose infusion rate (disintegrations per minute, dpm) to the specific activity of plasma glucose (dpm/mg) at the end of the basal period and during the final 30 min of steady state of the clamp, respectively. Endogenous glucose production was calculated by subtracting the glucose infusion rate from the whole-body insulin-stimulated glucose disposal. Whole body glycolysis rate was estimated by the ratio of delta ^3H_2O [dpm/(mL-min)] to the specific activity of plasma glucose (dpm/mg) at the end of the basal period and during the final 30 min of the clamp. Finally, glycogen synthesis rate was calculated by subtracting the glycolysis rate from the whole-body insulin-stimulated glucose disposal.

Liver Lipids Measurements. Tissue triglycerides were extracted using the method of Bligh and Dyer (32) and measured using a DCL triglyceride reagent (Diagnostic Chemicals). For DAG extraction, livers were homogenized in a buffer solution (20 mM Tris-HCl, 1 mM EDTA, 0.25 mM EGTA, 250 mM sucrose, 2 mM PMSF) containing a protease inhibitor mixture (Roche), and samples were centrifuged at 100,000 *g* for 1 h. The supernatants containing the cytosolic fraction were collected. DAG levels were then measured as previously described (9). Total cytosolic DAG content is expressed as the sum of individual species. Ceramide was measured as previously described (9). All lipid measurements were done in animals under basal conditions following a 6-h fast.

Liver Insulin Signaling. PKCε membrane translocation was assessed under basal conditions following a 6-h fast, and IRS-2 tyrosine phosphorylation was assessed at the end of the hyperinsulinemic-euglycemic clamps in liver protein extracts as previously described (31).

Total RNA Preparation, Real-Time Quantitative PCR Analysis, and Immunoblotting Analysis. Total RNA was extracted from frozen livers using RNeasy 96-kit (Qiagen), then 1 μg of RNA was reverse transcribed into cDNA with the use of the Quantitect RT kit (Qiagen) as per manufacturer's protocol. The abundance of transcripts was assessed by real-time PCR on a 7500 Real-Time PCR system (Applied Biosystems) with a SYBR Green detection system. Samples were run in duplicate for both the gene of interest and cyclophilin and data were normalized for the efficiency of amplification, as determined by a standard curve included on each run. Primers used are shown in Table S1. Liver proteins were extracted in radioimmunoprecipitation assay buffer as previously described (33), and protein concentration was determined by the bicinchoninic acid method (Pierce). Equal amounts of protein [30 μg; 50 μg for pAkt (Ser473) and Akt] were separated on a 4–12% gradient polyacrylamide gel (Invitrogen) and subsequently transferred to polyvinylidene fluoride membranes (Millipore) using a semidry transfer cell (Bio-Rad). After blocking in Tris-buffered saline-Tween 20 containing 5% nonfat dried milk, membranes were incubated overnight with primary antibodies (1:1,000 dilution; 1:500 for pAkt) for CHOP, BIP, phospho-eIF2α, and pAkt (Cell Signaling Technology). After further washings, membranes were incubated with horseradish peroxidase-conjugated secondary antibody (Bio-Rad) (1:3,000 dilution; 1:2,000 for pAkt and Akt) and visualized by enhanced chemiluminescent substrate (Pierce). Membranes were stripped and reblotted with anti-GAPDH antibody (Santa Cruz), total eIF2α, or Akt (Cell Signaling Technology) (1:1,000 dilution; 1:500 for Akt). Bands were then quantified using ImageJ (National Institutes of Health). All measurements were done in animals under basal conditions following a 6-h fast, except for pAkt and Akt, where measurements were also done at the end of the hyperglycemic-euglycemic clamps.

Statistical Analysis. Data are expressed as means ± SEM. Results were assessed using two-tailed unpaired Student's *t* test or one-way ANOVA (GraphPad; Prism 5). A *P* value less than 0.05 was considered significant.

ACKNOWLEDGMENTS. We thank Xian-Man Zhang, Mario Kahn, Xiaoxian Ma, and Aida Groszman for expert technical assistance and Dr. Robert Farese, Jr. for kindly providing us with the Liv-*DGAT2* mice. This work was supported by grants from the United States Public Health Service: R01 DK-40936 (to G.I.S.), U24 DK-059635 (to V.T.S. and G.I.S.), and P30 DK-45735 and a Veterans Affairs Merit Grant (to V.T.S.). F.R.J. was funded by Grant PASMP3-132563 from the Swiss National Science Foundation/Swiss Foundation for Grants in Biology and Medicine.

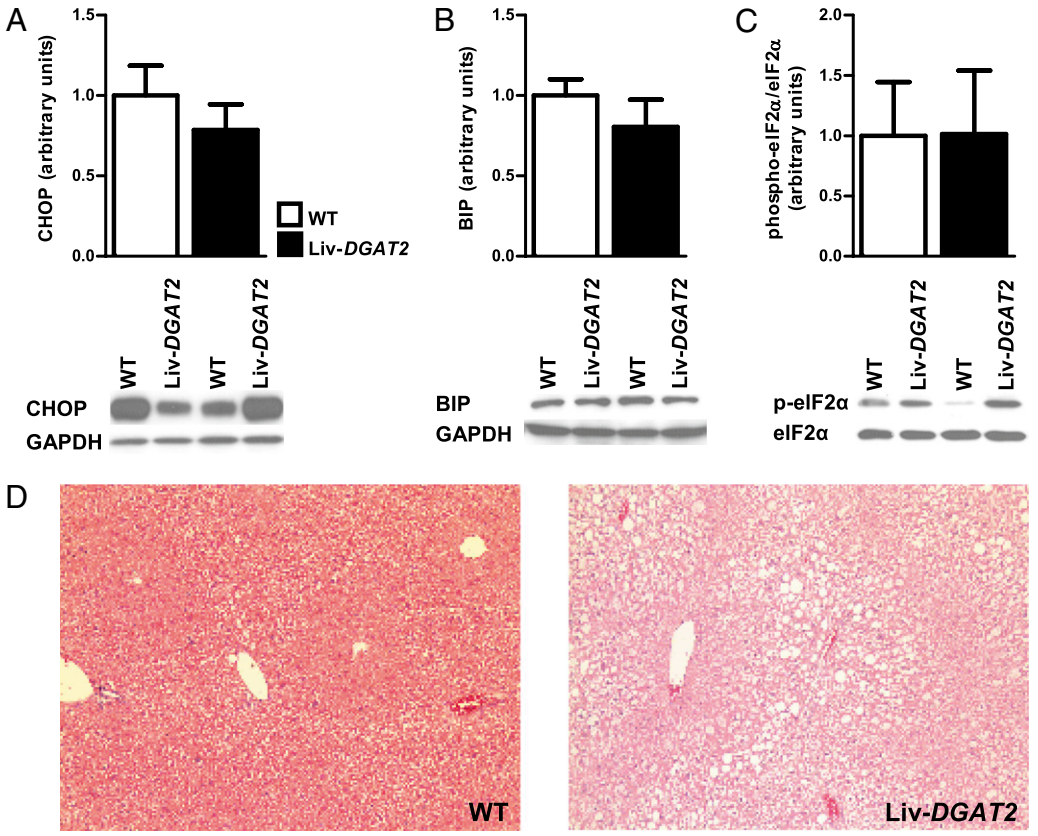

Fig. 3. Hepatic insulin resistance in Liv-*DGAT2* mice is not associated with ER stress or inflammation. (*A*) CHOP. (*B*) BIP. (*C*) phospho-eIF2α. (*D*) Histological evidence of NAFLD in Liv-*DGAT2* mice with predominantly macrovesicular pattern lipid infiltration and some degree of hepatic ballooning, without evident sign of inflammation (H&E staining, original magnification 100×). Data are represented as mean ± SEM.

1. Petersen KF, et al. (2005) Reversal of nonalcoholic hepatic steatosis, hepatic insulin resistance, and hyperglycemia by moderate weight reduction in patients with type 2 diabetes. *Diabetes* 54:603–608.
2. Angulo P (2002) Nonalcoholic fatty liver disease. *N Engl J Med* 346:1221–1231.
3. Samuel VT, Petersen KF, Shulman GI (2010) Lipid-induced insulin resistance: Unravelling the mechanism. *Lancet* 375:2267–2277.
4. Shulman GI (2000) Cellular mechanisms of insulin resistance. *J Clin Invest* 106:171–176.
5. Yki-Järvinen H (2010) Nutritional modulation of nonalcoholic fatty liver disease and insulin resistance: Human data. *Curr Opin Clin Nutr Metab Care* 13:709–714.
6. Fabbrini E, Sullivan S, Klein S (2010) Obesity and nonalcoholic fatty liver disease: Biochemical, metabolic, and clinical implications. *Hepatology* 51:679–689.
7. Utzschneider KM, Kahn SE (2006) Review: The role of insulin resistance in nonalcoholic fatty liver disease. *J Clin Endocrinol Metab* 91:4753–4761.
8. Browning JD, Cohen JC, Hobbs HH (2010) Patatin-like phospholipase domain-containing 3 and the pathogenesis and progression of pediatric nonalcoholic fatty liver disease. *Hepatology* 52:1189–1192.
9. Yu C, et al. (2002) Mechanism by which fatty acids inhibit insulin activation of insulin receptor substrate-1 (IRS-1)-associated phosphatidylinositol 3-kinase activity in muscle. *J Biol Chem* 277:50230–50236.
10. Erion DM, Shulman GI (2010) Diacylglycerol-mediated insulin resistance. *Nat Med* 16: 400–402.
11. Itani SI, Ruderman NB, Schmieder F, Boden G (2002) Lipid-induced insulin resistance in human muscle is associated with changes in diacylglycerol, protein kinase C, and IkappaB-alpha. *Diabetes* 51:2005–2011.
12. Griffin ME, et al. (1999) Free fatty acid-induced insulin resistance is associated with activation of protein kinase C theta and alterations in the insulin signaling cascade. *Diabetes* 48:1270–1274.
13. Holland WL, et al. (2007) Inhibition of ceramide synthesis ameliorates glucocorticoid-, saturated-fat-, and obesity-induced insulin resistance. *Cell Metab* 5:167–179.
14. Samuel VT, et al. (2007) Inhibition of protein kinase Cepsilon prevents hepatic insulin resistance in nonalcoholic fatty liver disease. *J Clin Invest* 117:739–745.
15. Monetti M, et al. (2007) Dissociation of hepatic steatosis and insulin resistance in mice overexpressing DGAT in the liver. *Cell Metab* 6:69–78.
16. Hotamisligil GS (2008) Inflammation and endoplasmic reticulum stress in obesity and diabetes. *Int J Obes (Lond)* 32(Suppl 7):S52–S54.
17. Taubes G (2009) Insulin resistance. Prosperity's plague. *Science* 325:256–260.
18. Ozcan U, et al. (2004) Endoplasmic reticulum stress links obesity, insulin action, and type 2 diabetes. *Science* 306:457–461.
19. Lazar MA (2005) How obesity causes diabetes: Not a tall tale. *Science* 307:373–375.
20. Hotamisligil GS (2006) Inflammation and metabolic disorders. *Nature* 444: 860–867.
21. Shimano H, et al. (1997) Isoform 1c of sterol regulatory element binding protein is less active than isoform 1a in livers of transgenic mice and in cultured cells. *J Clin Invest* 99: 846–854.
22. Postic C, Girard J (2008) Contribution of de novo fatty acid synthesis to hepatic steatosis and insulin resistance: Lessons from genetically engineered mice. *J Clin Invest* 118:829–838.
23. Stefan N, Kantartzis K, Häring HU (2008) Causes and metabolic consequences of fatty liver. *Endocr Rev* 29:939–960.
24. Yen CL, Stone SJ, Koliwad S, Harris C, Farese RV, Jr. (2008) Thematic review series: Glycerolipids. DGAT enzymes and triacylglycerol biosynthesis. *J Lipid Res* 49: 2283–2301.
25. Alkhouri N, Dixon LJ, Feldstein AE (2009) Lipotoxicity in nonalcoholic fatty liver disease: Not all lipids are created equal. *Expert Rev Gastroenterol Hepatol* 3:445–451.
26. Chavez JA, Summers SA (2010) Lipid oversupply, selective insulin resistance, and lipotoxicity: Molecular mechanisms. *Biochim Biophys Acta* 1801:252–265.
27. Feldstein AE (2010) Novel insights into the pathophysiology of nonalcoholic fatty liver disease. *Semin Liver Dis* 30:391–401.
28. Tilg H, Moschen AR (2008) Insulin resistance, inflammation, and non-alcoholic fatty liver disease. *Trends Endocrinol Metab* 19:371–379.
29. Nagle CA, Klett EL, Coleman RA (2009) Hepatic triacylglycerol accumulation and insulin resistance. *J Lipid Res* 50(Suppl):S74–S79.
30. Ayala JE, et al.; NIH Mouse Metabolic Phenotyping Center Consortium (2010) Standard operating procedures for describing and performing metabolic tests of glucose homeostasis in mice. *Dis Model Mech* 3:525–534.
31. Choi CS, et al. (2007) Suppression of diacylglycerol acyltransferase-2 (DGAT2), but not DGAT1, with antisense oligonucleotides reverses diet-induced hepatic steatosis and insulin resistance. *J Biol Chem* 282:22678–22688.
32. Bligh EG, Dyer WJ (1959) A rapid method of total lipid extraction and purification. *Can J Biochem Physiol* 37:911–917.
33. Jornayvaz FR, et al. (2010) A high-fat, ketogenic diet causes hepatic insulin resistance in mice, despite increasing energy expenditure and preventing weight gain. *Am J Physiol Endocrinol Metab* 299:E808–E815.